Journal of Quantitative Spectroscopy & Radiative Transfer 217 (2018) 329–337

Contents lists available at ScienceDirect

Journal of Quantitative Spectroscopy & Radiative Transfer

journal homepage: www.elsevier.com/locate/jqsrt

Ray optics for absorbing particles with application to ice crystals at near-infrared wavelengths

Hannakaisa Lindqvist[a,*], Julia Martikainen[b], Jukka Räbinä[b,c], Antti Penttilä[b], Karri Muinonen[b,d]

[a] Space and Earth Observation Centre, Finnish Meteorological Institute (FMI), P.O. Box 503, 00101 Helsinki, Finland
[b] Department of Physics, University of Helsinki, P.O. Box 64, 00014, Finland
[c] Faculty of Information Technology, University of Jyvaskyla, P.O. Box 35, 40014, Finland
[d] National Land Survey of Finland, Finnish Geospatial Research Institute (FGI), Geodeetinrinne 2, 02430 Masala, Finland

ARTICLE INFO

Article history:
Received 3 February 2018
Revised 17 May 2018
Accepted 6 June 2018
Available online 7 June 2018

Keywords:
Absorbing media
Inhomogeneous waves
Ice crystals
Ray optics
Scattering

ABSTRACT

Light scattering by particles large compared to the wavelength of incident light is traditionally solved using ray optics which considers absorption inside the particle approximately, along the ray paths. To study the effects rising from this simplification, we have updated the ray-optics code SIRIS to take into account the propagation of light as inhomogeneous plane waves inside an absorbing particle. We investigate the impact of this correction on traditional ray-optics computations in the example case of light scattering by ice crystals through the extended near-infrared (NIR) wavelength regime. In this spectral range, ice changes from nearly transparent to opaque, and therefore provides an interesting test case with direct connection and applicability to atmospheric remote-sensing measurements at NIR wavelengths. We find that the correction for inhomogeneous waves systematically increases the single-scattering albedo throughout the NIR spectrum for both randomly-oriented, column-like hexagonal crystals and ice crystals shaped like Gaussian random spheres. The largest increase in the single-scattering albedo is 0.042 for hexagonal crystals and 0.044 for Gaussian random spheres, both at $\lambda = 2.725$ μm. Although the effects on the 4×4 scattering-matrix elements are generally small, the largest differences are seen at 2.0 μm and 3.969 μm wavelengths where the correction for inhomogeneous waves affects mostly the backscattering hemisphere of the depolarization-connected P_{22}/P_{11}, P_{33}/P_{11}, and P_{44}/P_{11}. We evaluated the correction for inhomogeneous waves through comparisons against the discrete exterior calculus (DEC) method. We computed scattering by hexagonal ice crystals using the DEC, a traditional ray-optics code (SIRIS3), and a ray-optics code with inhomogeneous waves (SIRIS4). Comparisons of the scattering-matrix elements from SIRIS3 and SIRIS4 against those from the DEC suggest that consideration of the inhomogeneous waves brings the ray-optics solution generally closer to the exact result and, therefore, should be taken into account in scattering by absorbing particles large compared to the wavelength of incident light.

1. Introduction

Geometric optics and its descriptive concept of light rays offers a straightforward yet approximate methodology for various optics applications that consider reflections by surfaces and light scattering by small particles. In the latter case, specifically, the geometric-optics approximation combined with diffraction form the ray-optics solution. Despite recent exploding development in computational light scattering in both availability of resources and more advanced methods, most notably those based on physical optics [1,2], ray optics continues to be a frequently used method for solving scattering by particles much larger than the wavelength of incident light.

An important example of such scatterers are atmospheric ice crystals. These particles are continuously present in the atmosphere as constituents of tropospheric cirrus clouds, which cover approximately one third of the surface of the Earth at any given time, based on satellite observations [3,4]. The majority of the radiative effects originating from these clouds (multiple scattering of sunlight and thermal radiation) ultimately depends on the single-scattering properties of the ice crystals [5], in addition to their size and shape distributions within the cloud. These single-

* Corresponding author.
E-mail address: hannakaisa.lindqvist@fmi.fi (H. Lindqvist).

https://doi.org/10.1016/j.jqsrt.2018.06.005

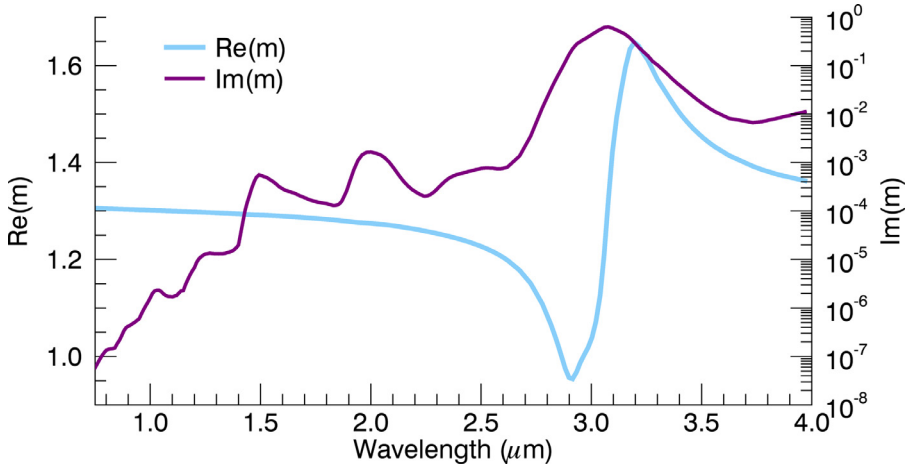

Fig. 1. Spectral dependence of the complex refractive index m of ice at near-infrared wavelengths, using data from Warren and Brandt [36].

scattering properties have most frequently been solved using ray optics. Therefore, the evolution and advancements in the ray-optics methodology intertwine with the history of solving light scattering by ice crystals. Studies on scattering by hexagonal and rectangular parallelepiped crystals in the geometric-optics approximation were initially carried out by Jacobowitz [6], Wendling et al. [7], Cai and Liou [8], as well as Liou et al. [9,10] and Takano and Jayaweera [11]. These studies mainly focused on randomly oriented crystals and the angular characteristics of scattered intensity and linear polarization for natural incident light. Takano and Jayaweera provided, however, a full 4×4 Mueller scattering matrix for hexagonal ice crystals.

The aforedescribed geometric-optics treatments were extended to parallelepiped crystals with interfacial angles different from right angles, that is, to monoclinic and triclinic crystals, by Muinonen et al. [12]. Peltoniemi et al. [13] provided a Markov-chain ray-tracing method for stochastically rough particles. Muinonen et al. [14], in their studies for scattering by Gaussian random particles, provided a general geometric-optics treatment for arbitrary shapes specified in three-dimensional space. At the same time, Macke et al. [15] devised a geometric-optics treatment for crystal particles described as a Koch fractal. The largely independent geometric-optics ray tracers by Muinonen et al. [14] and Macke et al. [15] were compared in detail for the Koch fractal [16]. The ray tracers were found to agree well. More recent work on the geometric-optics approximation has been carried out using general triangular discretization of the particle shapes (e.g., [17,18]). Beyond geometric optics, there is promising progress in establishing the physical optics approximation as a practical computational tool for light scattering by nonspherical particles (e.g., [1,19,20]).

There are large numbers of applications of the geometric-optics method. For example, first, Nousiainen and Muinonen assessed the scattering characteristics of randomly oscillating raindrops in the visible range of wavelengths [21]. Second, Muinonen and Erkkilä ([22]; see also [23]) studied the effect of large-scale surface roughness on the scattering characteristics, with the help of a concave hull of an arbitrary irregular particle shape. Third, Virkki and Muinonen [24] studied microwave scattering by boulders, in their quest for understanding the radar backscattering characteristics of asteroids and other small Solar System bodies. Fourth, the traditional geometric-optics treatment has been combined with radiative transfer for particles including internal or external diffuse scatterers (e.g., [18,25,26]).

The geometric-optics method can be applied to absorbing media; however, traditionally absorption within the particle has been solved approximately, neglecting the inhomogeneity of the waves in the medium. Already in 1930, Epstein [27] pointed out that waves in absorbing media propagate as inhomogeneous waves, i.e., have planes of constant amplitude and constant phase, which do not generally coincide. This has two consequences in geometric optics: (1) Snel's law and the Fresnel equations that determine the reflections and refractions at the interfaces should not be used in their traditional forms that only account for real-valued variables, and (2) attenuation of radiation inside the medium should not be calculated using a simple exponential attenuation along the ray path, as this does not take into account the inhomogeneous nature of the plane waves. These issues have been briefly recognized but not conclusively addressed in otherwise extensive textbooks on light scattering (e.g., [28–31]). The work by Dupertuis et al. [32] on geometric optics in absorbing media introduces the concept of a "deflection angle", i.e., an angle between the planes of incidence and refraction, which serves as an example on the unresolved questions surrounding the topic. Chang et al. [33] have derived concise expressions for Snel's law and the Fresnel equations in an absorbing medium based on [32], and showed analytical ray-tracing results for a two-dimensional wedge of absorbing medium and Monte Carlo computations for an absorbing rough surface. Parallel formalisms that consider inhomogeneous waves in geometric-optics approximation have been presented by Yang et al. [34] and Yang and Liou [35]. However, the implications of the correction have not been quantified with respect to the traditional geometric-optics computations for scattering by ice crystals.

In this paper, we update the ray-tracing code SIRIS [18] to consider inhomogeneous plane waves by implementing the methodology presented in [33], and then apply the updated SIRIS4 code to quantify the effects of inhomogeneous waves on light scattering by ice crystals. For visible light, ice crystals are in practice nearly transparent with an imaginary part of the refractive index $\mathrm{Im}(m) \approx 10^{-8}$ [36]. However, in the extended near-infrared (NIR) spectral region from 0.75 μm to 4.0 μm, both $\mathrm{Re}(m)$ and $\mathrm{Im}(m)$ change significantly as depicted in Fig. 1. Therefore, this spectral region provides an interesting sensitivity test environment with a direct connection and applicability to a variety of atmospheric remote-sensing measurements at the NIR wavelengths — including not only instruments measuring cirrus clouds but also atmospheric composition retrievals with high accuracy requirements, such as retrievals of trace gases (e.g., carbon dioxide, methane). We evaluate the ray-optics results through comparisons to exact scattering computations from the discrete exterior calculus (DEC) [37–39].

2. Ray optics with inhomogeneous plane waves

Traditional ray-optics approximation is based on the plane wave solution to the Maxwell equations, where the phases of the waves can be omitted based on particle size being much larger than the wavelength λ of incident light. Incident wave is thus treated as a collection of parallel rays that propagate in the direction of the normal to the plane of constant phase. The interaction of these rays with a medium is modeled as a sequence of reflections and refractions at the interfaces, determined by Snel's law and the Fresnel equations. The plane wave $\mathbf{E}(\mathbf{r}, t)$ is of the form

$$\mathbf{E}(\mathbf{r}, t) = \mathbf{E}_0 \exp(\mathrm{i}\mathbf{k}\cdot\mathbf{r} - \mathrm{i}\omega t). \tag{1}$$

In an absorbing medium, $\mathbf{k}$ is the complex wave vector, $\mathbf{k} = k_0(N\hat{\mathbf{e}} + \mathrm{i}K\hat{\mathbf{f}})$, where $k_0 = \omega/c$, and N and K are interpreted as medium-specific, apparent refractive indices [33]. Substituting $\mathbf{k}$, we can further express Eq. (1) as

$$\mathbf{E}(\mathbf{r}, t) = \mathbf{E}_0 \exp(-k_0 K\hat{\mathbf{f}}\cdot\mathbf{r}) \exp(\mathrm{i}k_0 N\hat{\mathbf{e}}\cdot\mathbf{r} - \mathrm{i}\omega t), \tag{2}$$

which describes inhomogeneous plane waves where the surfaces of constant amplitude are perpendicular to $\hat{\mathbf{f}}$ and the surfaces of constant phase are perpendicular to $\hat{\mathbf{e}}$. The angle between these vectors is α, and thus $\cos\alpha = \hat{\mathbf{e}}\cdot\hat{\mathbf{f}}$. In traditional geometric-optics considerations, it is generally assumed that $\alpha = 0°$, $\hat{\mathbf{e}} \parallel \hat{\mathbf{f}}$, i.e., the plane waves are homogeneous and absorption is considered in the direction of wave propagation.

The generalized Snel's law for waves in absorbing media can be derived from the boundary conditions for the phases of the plane waves at the interface of two media (subscripts 1 and 2) [33]:

$$N_1 \sin\vartheta_\mathrm{i} = N_2 \sin\vartheta_\mathrm{t}, \qquad K_1 \sin\psi_\mathrm{i} = K_2 \sin\psi_\mathrm{t}. \tag{3}$$

Here, ϑ and ψ are real-valued angles of $\hat{\mathbf{e}}$ and $\hat{\mathbf{f}}$ from the normal of the surface, respectively, for incident (i) and transmitted (t) rays. The propagation directions $\hat{\mathbf{e}}_\mathrm{t}$ and $\hat{\mathbf{f}}_\mathrm{t}$ for the refracted waves are solved using Eqs. (3).

The Stokes vectors for incident and scattered light, $\mathbf{I}_\mathrm{inc}$ and $\mathbf{I}_\mathrm{sca}$, describe the polarization state of radiation and are related through the 4×4 scattering phase matrix $\mathbf{P}$,

$$\mathbf{I}_\mathrm{sca} = \frac{\sigma_\mathrm{sca}}{4\pi r^2}\mathbf{P}\cdot\mathbf{I}_\mathrm{inc}. \tag{4}$$

Here, $\mathbf{P}$ is normalized according to the phase function, $\mathbf{P}_{11}$:

$$\int_{4\pi} \mathbf{P}_{11}\,\mathrm{d}\Omega = 4\pi. \tag{5}$$

The scattering cross section σ_sca describes the total scattered power. In the ray-optics approximation, it can be divided into components that are solved through geometric optics ($\sigma^\mathrm{G}_\mathrm{sca}$) and forward diffraction ($\sigma^\mathrm{D}_\mathrm{sca}$):

$$\sigma_\mathrm{sca} = \sigma^\mathrm{G}_\mathrm{sca} + \sigma^\mathrm{D}_\mathrm{sca}. \tag{6}$$

Conversely, absorption σ_abs originates from the geometric-optics component only. The extinction cross section σ_ext describes the total power removed from the incident radiation through scattering and absorption,

$$\sigma_\mathrm{ext} = \sigma_\mathrm{sca} + \sigma_\mathrm{abs}. \tag{7}$$

The relative contributions of scattering and absorption can be characterized by the single-scattering albedo ϖ,

$$\varpi = \frac{\sigma_\mathrm{sca}}{\sigma_\mathrm{ext}} = \frac{\sigma^\mathrm{G}_\mathrm{sca} + \sigma^\mathrm{D}_\mathrm{sca}}{\sigma_\mathrm{ext}}. \tag{8}$$

In the geometric-optics component, we follow the treatment by Muinonen et al. [14], where a 4×4 Mueller matrix $\mathbf{M}$ is related to every ray. At an interface, we solve for the Mueller matrices of the reflected and refracted rays using the Fresnel reflection and transmission matrices, $\mathbf{R}$ and $\mathbf{T}$:

$$\mathbf{M}_\mathrm{r} = \mathbf{R}\cdot\mathbf{K}\cdot\mathbf{M}_\mathrm{i} \tag{9}$$

$$\mathbf{M}_\mathrm{t} = \mathbf{T}\cdot\mathbf{K}\cdot\mathbf{M}_\mathrm{i}. \tag{10}$$

Here, $\mathbf{K}$ is the rotation to the plane of incidence. To solve for $\mathbf{K}$, we first define a set of complex, orthogonal basis vectors

$$\hat{\mathbf{h}}_1 = \frac{\mathbf{k}\times\mathbf{n}}{\sqrt{(\mathbf{k}\times\mathbf{n})^2}}, \qquad \hat{\mathbf{h}}_2 = \frac{\hat{\mathbf{h}}_1\times\mathbf{k}}{k_0 m}. \tag{11}$$

$\mathbf{K}$ describes the rotation of the field vectors from the basis $(\hat{\mathbf{h}}_1, \hat{\mathbf{h}}_2)$ to $(\hat{\mathbf{h}}'_1, \hat{\mathbf{h}}'_2)$:

$$\mathbf{K} = \begin{bmatrix} \frac{1}{2}(J_1J_1^* + J_2J_2^* + J_3J_3^* + J_4J_4^*) & \frac{1}{2}(-J_1J_1^* + J_2J_2^* + J_3J_3^* - J_4J_4^*) \\ \frac{1}{2}(-J_1J_1^* + J_2J_2^* - J_3J_3^* + J_4J_4^*) & \frac{1}{2}(J_1J_1^* + J_2J_2^* - J_3J_3^* - J_4J_4^*) \\ \mathrm{Re}(J_1J_4^* + J_3J_2^*) & \mathrm{Re}(-J_1J_4^* + J_3J_2^*) \\ \mathrm{Im}(J_1^*J_4 + J_3^*J_2) & \mathrm{Im}(-J_1^*J_4 + J_3^*J_2) \end{bmatrix}$$

$$\begin{bmatrix} \mathrm{Re}(J_1J_3^* + J_4J_2^*) & -\mathrm{Im}(J_1^*J_3 + J_4^*J_2) \\ \mathrm{Re}(-J_1J_3^* + J_4J_2^*) & -\mathrm{Im}(-J_1^*J_3 + J_4^*J_2) \\ \mathrm{Re}(J_1J_2^* + J_3J_4^*) & -\mathrm{Im}(J_1^*J_2 - J_3^*J_4) \\ \mathrm{Im}(J_1^*J_2 + J_3^*J_4) & \mathrm{Re}(J_1J_2^* - J_3J_4^*) \end{bmatrix}, \tag{12}$$

where $J_1 = \hat{\mathbf{h}}_1\cdot\hat{\mathbf{h}}'_1, J_2 = \hat{\mathbf{h}}_2\cdot\hat{\mathbf{h}}'_2, J_3 = \hat{\mathbf{h}}_2\cdot\hat{\mathbf{h}}'_1$, and $J_4 = \hat{\mathbf{h}}_1\cdot\hat{\mathbf{h}}'_2$. The Fresnel reflection and transmission matrices in Eqs. (9)–(10) are

$$\mathbf{R} = \frac{1}{2}\begin{bmatrix} r_\parallel r_\parallel^* + r_\perp r_\perp^* & r_\parallel r_\parallel^* - r_\perp r_\perp^* & 0 & 0 \\ r_\parallel r_\parallel^* - r_\perp r_\perp^* & r_\parallel r_\parallel^* + r_\perp r_\perp^* & 0 & 0 \\ 0 & 0 & 2\,\mathrm{Re}(r_\parallel r_\perp^*) & 2\,\mathrm{Im}(r_\parallel r_\perp^*) \\ 0 & 0 & -2\,\mathrm{Im}(r_\parallel r_\perp^*) & 2\,\mathrm{Re}(r_\parallel r_\perp^*) \end{bmatrix}, \tag{13}$$

$$\mathbf{T} = \frac{1}{2}\begin{bmatrix} t_\parallel t_\parallel^* + t_\perp t_\perp^* & t_\parallel t_\parallel^* - t_\perp t_\perp^* & 0 & 0 \\ t_\parallel t_\parallel^* - t_\perp t_\perp^* & t_\parallel t_\parallel^* + t_\perp t_\perp^* & 0 & 0 \\ 0 & 0 & 2\,\mathrm{Re}(t_\parallel t_\perp^*) & 2\,\mathrm{Im}(t_\parallel t_\perp^*) \\ 0 & 0 & -2\,\mathrm{Im}(t_\parallel t_\perp^*) & 2\,\mathrm{Re}(t_\parallel t_\perp^*) \end{bmatrix}, \tag{14}$$

where $r_\parallel$, $r_\perp$, $t_\parallel$, and $t_\perp$ are the Fresnel coefficients (a minor typo corrected from [33, Eq. (14)])

$$r_\parallel = \frac{m_2^2 k_i - m_1^2 k_t}{m_2^2 k_i + m_1^2 k_t}, \qquad r_\perp = \frac{k_i - k_t}{k_i + k_t}$$
$$t_\parallel = \frac{2m_1 m_2 k_i}{m_2^2 k_i + m_1^2 k_t}, \qquad t_\perp = \frac{2k_i}{k_i + k_t}.$$

Here, m_1 and m_2 are the complex refractive indices of the two media, and

$k_i = k_0(N_1\cos\vartheta_i + \mathrm{i}K_1\cos\psi_i)$ and $k_t = k_0(N_2\cos\vartheta_t + \mathrm{i}K_2\cos\psi_t)$.

For the diffraction component of the ray-optics solution, we follow the treatment by Muinonen et al. [14] and apply it to both Gaussian random spheres and hexagonal crystals. The forward diffraction is calculated using the Kirchhoff approximation, where the ensemble-averaged diffraction phase matrix is

$$\langle \mathbf{P}_{\mathrm{D}}(\theta)\rangle \propto \frac{k^2}{4\pi\langle A\rangle}\langle |u(\theta,\varphi)|^2\rangle (1+\cos\theta)^2\mathbf{1}, \tag{15}$$

$$u(\theta,\varphi) = \int_0^{2\pi} \mathrm{d}\varphi' \int_0^{r(\varphi')} \mathrm{d}r' \exp[-ikr'\sin\theta\cos(\varphi-\varphi')]. \tag{16}$$

Here, $\mathbf{1}$ is the 4×4 identity matrix, θ is the scattering angle (i.e., the angle between the incident and scattered radiation) and $r(\varphi')$ describes the silhouette perimeter of a sample ice crystal in polar coordinates.

Finally, the phase matrix from the ray-optics solution is

$$\mathbf{P}(\theta) = \frac{1}{\sigma_{\mathrm{sca}}}(\sigma^{\mathrm{G}}_{\mathrm{sca}}\mathbf{P}_{\mathrm{G}}(\theta) + \sigma^{\mathrm{D}}_{\mathrm{sca}}\mathbf{P}_{\mathrm{D}}(\theta)). \tag{17}$$

3. Computational aspects

3.1. Ray-optics code SIRIS4

We implemented the appropriate treatment of inhomogeneous plane waves presented in Section 2 in a traditional ray-optics code SIRIS [14] and, with these updates, thus introduce the version SIRIS4. As for the geometric-optics part, SIRIS4 is built to follow and update the changes in the 4×4 Mueller matrix instead of the Stokes parameters associated with each ray, which was the method in the preceding version, SIRIS3 [18]. In the code, the surface of the particle is presented with a triangle mesh. In principle, this allows the consideration of arbitrary shapes, provided that the general limitations set by the geometric-optics method are satisfied. Thus far, we have implemented the shapes of a hexagonal prism and the Gaussian random sphere [14]. While the former is a convex shape, the latter is generally non-convex; thus, rays that are reflected (or twice transmitted) may re-enter the surface of the non-convex particle.

For the computations, we included 1,000,000 rays, which were traced through multiple sequences of reflections and refractions branching the ray until the relative flux of the branch was below 10^{-4}. Another criterion was to allow a maximum of 20 internal reflections. These values were found sufficient through multiple test runs.

3.2. Discrete exterior calculus (DEC)

Evaluation computations for the hexagonal ice crystals were performed with a code employing discrete exterior calculus (DEC) [37–39]. The solution method is a generalization of the finite difference techniques such as the finite-difference time-domain (FDTD) [40,41] or finite integration techniques (FIT) [42].

The integrated values of electric and magnetic fields (denoted by column vectors $\mathbf{e}$ and $\mathbf{h}$) are assigned on edge elements of 3-dimensional primal and dual meshes, respectively. The counterparts of the curl operators are denoted by *discrete exterior derivatives* d_1 and d_1^T, where the incidence matrix d_1 consists of the relative orientations ($+1$ or -1) of each connected pair of edge and face. The material relations are described by diagonal matrices $\star\epsilon$, $\star\sigma$, and $\star\mu$. These *discrete Hodge operators* are the only source for numerical error. The Maxwell equations after spatial DEC discretization are

$$\begin{aligned} \star\epsilon\,\partial_t\mathbf{e} + \star\sigma\,\mathbf{e} - \mathrm{d}_1^T\mathbf{h} &= \mathbf{j},\\ \star\mu\,\partial_t\mathbf{h} + \mathrm{d}_1\mathbf{e} &= 0. \end{aligned}$$

The ice crystals are large compared to the wavelength λ, so the solution is highly dependent on numerical dispersion. With appropriate mesh structure and discrete Hodge terms, the numerical dispersion is nearly eliminated [38,39]. Due to the hexagonal base, we discretize the ice crystals using the Z-grid, which is one of the tetrahedrally close-packed structures. The object is surrounded by one wavelength thick perfectly matched layer (PML). Discretization level is tuned such that there exist at least 6000 unknowns per λ^3.

The time-harmonic solution is obtained using time-harmonic source terms and performing forward-in-time integration with non-uniform leapfrog strategy. From the near-field solution, we compute the far-field Mueller matrices. Averaged Mueller matrices are calculated using 1100–3200 wave propagation directions and 128 azimuth orientations for each direction. The solution method parallelizes nearly perfectly. Thus, we simultaneously exploited 576–2400 parallel CPUs (Intel Xeon E5-2670 at 2.60 GHz). In total, the computations of this paper took tens of CPU years.

4. Results and discussion

We demonstrate the effect of inhomogeneous plane waves on ray-optics computations through scattering by ice crystals in the NIR wavelengths. In the following demonstration, two ice crystal shape models are considered: hexagonal columns and Gaussian random spheres. These example computations cover the extended near-infrared spectral region, namely wavelengths from 0.75 μm to 3.969 μm, in intervals of approximately 0.02 μm because, in this region, the complex refractive index of ice has a strong spectral variability, as shown in Fig. 1. In our computations, we used the refractive index of ice tabulated and published by Warren and Brandt [36].

4.1. Hexagonal column ice crystals

We studied scattering by randomly oriented hexagonal column ice crystals that are common constituents of tropospheric cirrus clouds [e.g., 43]. The length of the crystal was set to 100 μm and, following the column ice crystal aspect ratio used by [44], the width of one hexagonal edge was 34.8 μm.

The correction for inhomogeneous plane waves implemented in SIRIS4 was first evaluated through comparisons of SIRIS3 and SIRIS4 computations against the results from the DEC, which can be considered as an exact computational light-scattering method. We limited these computations to two wavelengths, $\lambda = 2.000$ μm and $\lambda = 3.969$ μm. At these wavelengths, the differences between the scattering matrices from SIRIS3 and SIRIS4 were maximal to facilitate evaluation. The SIRIS3, SIRIS4, and the DEC results for hexagonal column ice crystals are shown in Figs. 2 and 3. For quantitative evaluation, the root-mean-square errors (RMSE) were calculated following

$$\mathrm{RMSE} = \sqrt{\frac{1}{n_\theta}\sum_{\theta=20^\circ}^{160^\circ}(P_{\mathrm{R}} - P_{\mathrm{DEC}})^2}, \tag{18}$$

where n_θ is the number of the scattering angle bins in the interval, and P_{R} refers to ray-optics computations and is $P_{\mathrm{R}} = P_{ij}/P_{11}$ except for the phase function $P_{\mathrm{R}} = P_{11}$, and similarly for P_{DEC} which denotes the DEC computations. Due to the computational challenges near the direct forward and backscattering directions, we considered scattering angles $\theta \in [20^\circ, 160^\circ]$ in the comparisons. The RMSE results are listed in Table 1. At $\lambda = 2.0$ μm, the RMSE values were smaller for SIRIS4 than SIRIS3 except for P_{22}/P_{11}, suggesting that the correction for inhomogeneous plane waves brings the ray-optics computations closer to the exact result. At $\lambda = 3.969$ μm, SIRIS4 agreed better with DEC results for the following four scattering-matrix elements: P_{21}/P_{11}, P_{22}/P_{11}, P_{33}/P_{11} and P_{44}/P_{11}. As the ray-optics methods (SIRIS3 and SIRIS4) are fundamentally approximate and different from exact methods such as the DEC, a perfect agreement cannot be expected. Nevertheless, evaluation of the RMSE at these two wavelengths suggests that

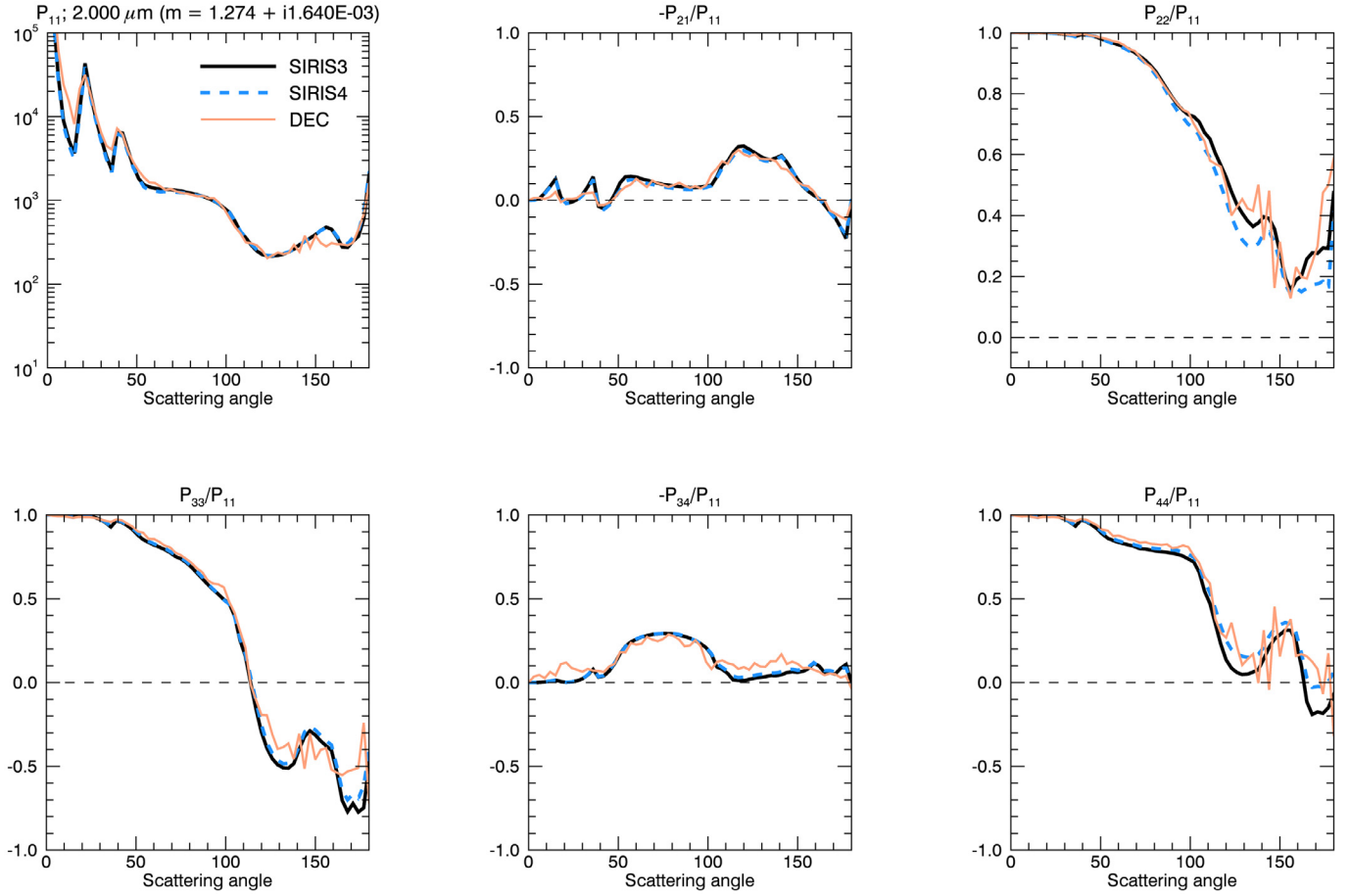

Fig. 2. Angular dependence of scattering by hexagonal ice crystals at $\lambda = 2.00$ μm computed using traditional ray optics (SIRIS3), ray optics with inhomogeneous waves (SIRIS4), and an exact method (DEC).

Table 1
The root-mean-square errors (RMSE) for traditional ray optics (SIRIS3) and ray optics with inhomogeneous waves (SIRIS4) with respect to the DEC.

	RMSE, $\lambda = 2.0$ μm		RMSE, $\lambda = 3.969$ μm	
	SIRIS3	SIRIS4	SIRIS3	SIRIS4
P_{11}	1731.8	1222.0	180.1	191.4
P_{21}/P_{11}	0.032	0.028	0.11	0.092
P_{22}/P_{11}	0.045	0.057	0.054	0.025
P_{33}/P_{11}	0.070	0.067	0.12	0.054
P_{34}/P_{11}	0.056	0.050	0.040	0.057
P_{44}/P_{11}	0.089	0.076	0.18	0.058

SIRIS4 with inhomogeneous waves agrees generally better with the DEC than the traditional ray optics (SIRIS3).

After evaluation, we investigated the sensitivity of scattering by ice crystals to the inhomogeneous waves throughout the extended NIR spectral region. The changes in the angular-dependent scattering-matrix elements were generally very small. Differences occurred around $\lambda = 1.5$ μm and $\lambda = 2.0$ μm which coincided with two separate absorption maxima for ice (Fig. 1). The most sensitive elements were P_{22}/P_{11}, P_{33}/P_{11}, and P_{44}/P_{11}, mainly at large scattering angles. Ice has also a broad absorption feature peaking at $\lambda = 3.07$ μm; however, this does not cause differences between SIRIS3 and SIRIS4 results because most of the scattered radiation originates from surface reflection as the refracted rays are attenuated due to the strong absorption inside the particle. When approaching the longer-wave end of the NIR region, scattering is again more sensitive to the treatment of inhomogeneous waves, which can be seen in Fig. 3 where all scattering-matrix elements are affected, including the phase function and the intensity of the halo phenomena. Thus, it appears that a sensitivity region for inhomogeneous waves in scattering can be identified between negligible absorption and surface reflection (where the correction is minimal in both cases); this is roughly at the wavelengths where $\mathrm{Im}(m) \in [2.0 \cdot 10^{-4}, 1.0 \cdot 10^{-2}]$ but depends on $\mathrm{Re}(m)$ as well as on the size of the particle.

In addition to the angular dependence on scattering through the NIR wavelengths, we evaluated the impact of the inhomogeneous waves on the single-scattering albedo ϖ. We found a small but systematic increase in ϖ throughout the NIR region (Fig. 4, left). The largest absolute increase was 0.042 at $\lambda = 2.725$ μm, and the largest relative increase was 6.3% at $\lambda = 2.778$ μm. The systematic increase of ϖ can be explained by the effectively shorter path length of the rays in the absorbing medium when inhomogeneous waves are considered.

4.2. Gaussian-random-sphere ice particles

We investigated light scattering by randomly oriented Gaussian-random-sphere ice particles large compared to the wavelength of the incident light. The Gaussian random sphere is parameterized by the mean radius a and coefficients C_l which are further parameterized by the power-law index ν and the standard deviation of the radius σ. The average volume depends on σ and a [45]:

$$\langle V \rangle = \frac{4}{3}\pi a^3 (1+\sigma^2)^3. \tag{19}$$

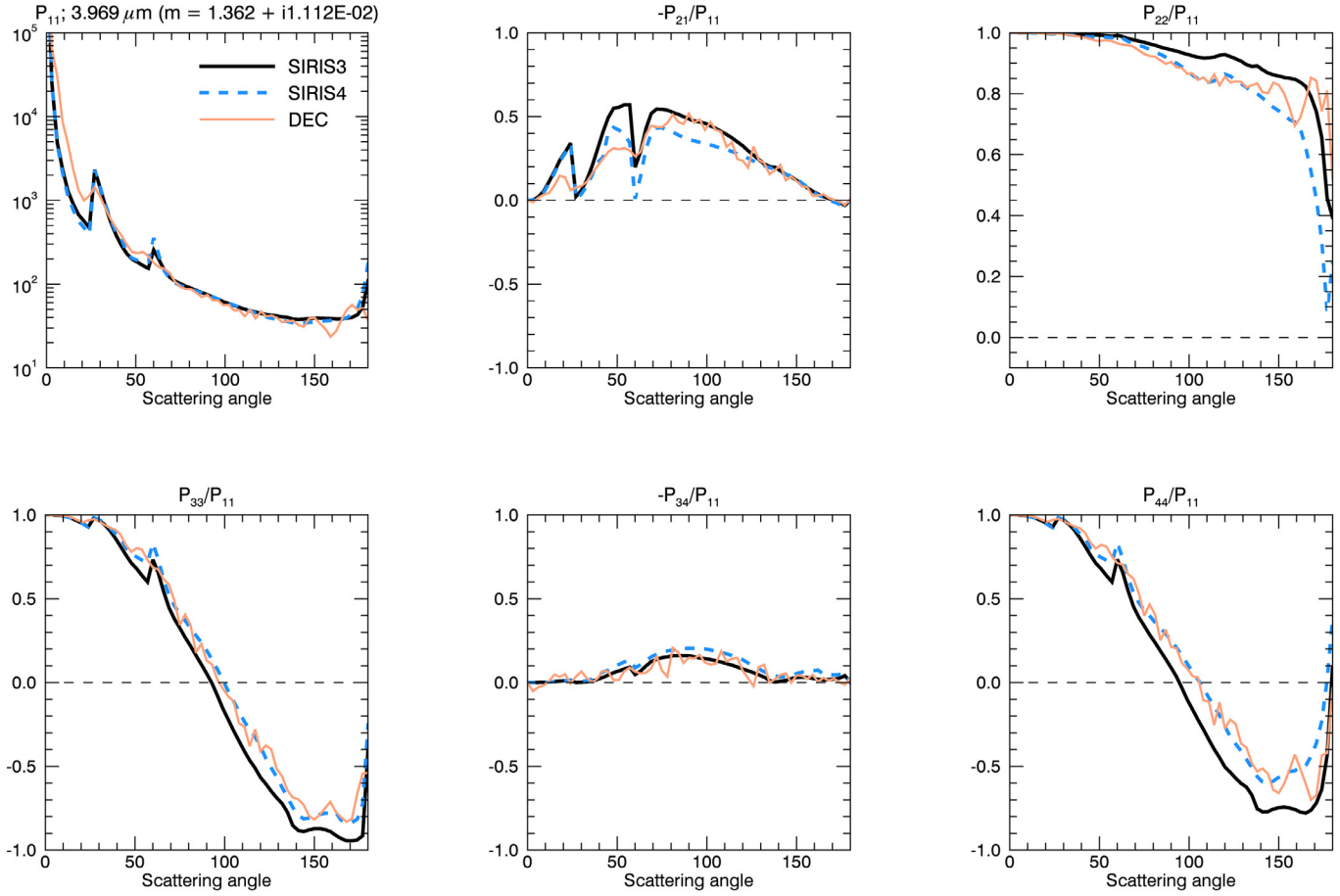

Fig. 3. Angular dependence of scattering by hexagonal ice crystals at $\lambda = 3.969$ μm computed using traditional ray optics (SIRIS3), ray optics with inhomogeneous waves (SIRIS4), and an exact method (DEC).

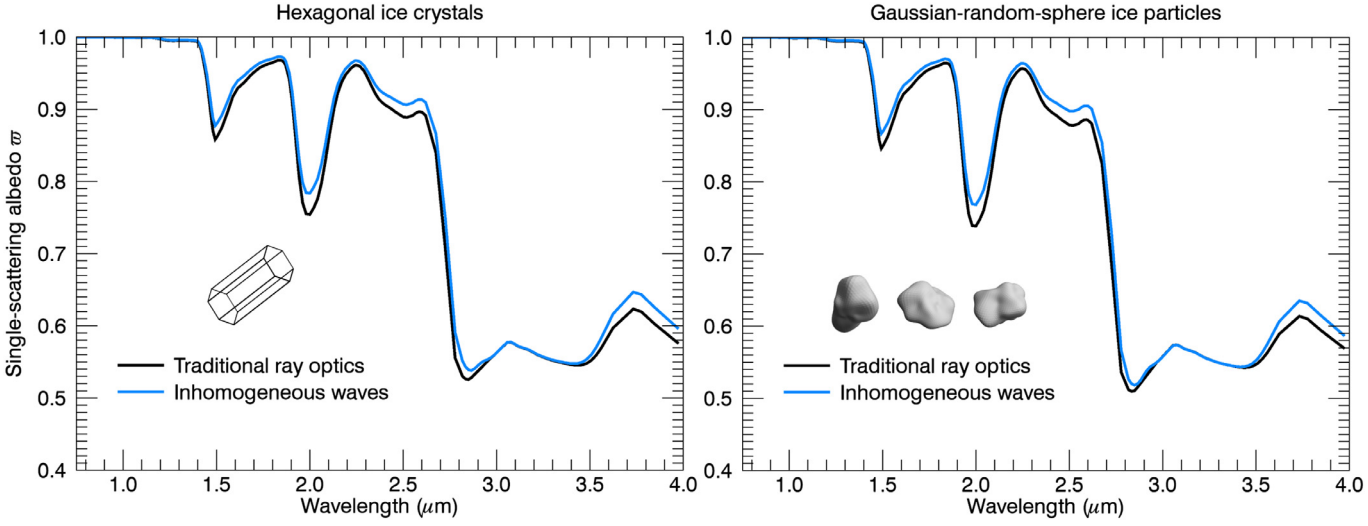

Fig. 4. Spectral dependence of the single-scattering albedo ϖ for hexagonal ice crystals (left) and Gaussian-random-sphere ice particles (right) in the NIR region using traditional ray optics (SIRIS3) and ray optics with inhomogeneous plane waves (SIRIS4).

The detailed mathematical presentation for the shape of the Gaussian random sphere is described in [18], and the shape model has been previously applied to atmospheric ice crystals by, e.g., [26].

For the computations, we used $\nu = 3.0$ and $\sigma = 0.17$. The mean radius a for the Gaussian random spheres was set to 41.674 μm, which was obtained by utilizing Eq. (19) and setting the volume of the Gaussian random sphere and the volume of the hexagonal column ice crystal (see Section 4.1) equal. Fig. 5 shows illustrations of the different shapes used in the computations.

We carried out computations at the NIR wavelength region with the SIRIS4 code, which accounts for inhomogeneous waves, and the traditional ray-optics code SIRIS3 [18]. We then compared the differences of the computed scattering matrices and single-scattering albedos ϖ. As shown in Fig. 4 (right), the ϖ calculated using in-

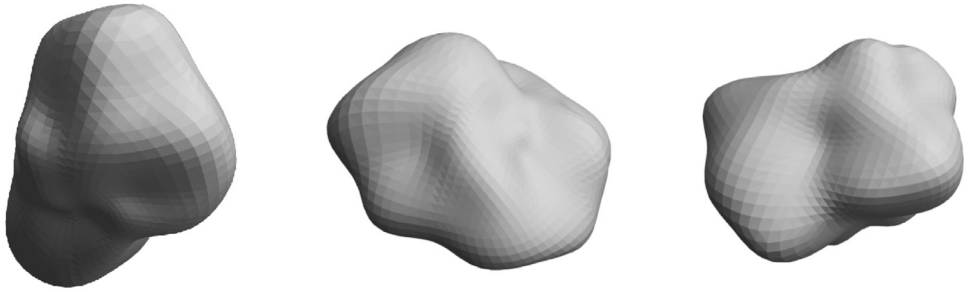

Fig. 5. Example shapes of the computed Gaussian-random-sphere ice particles.

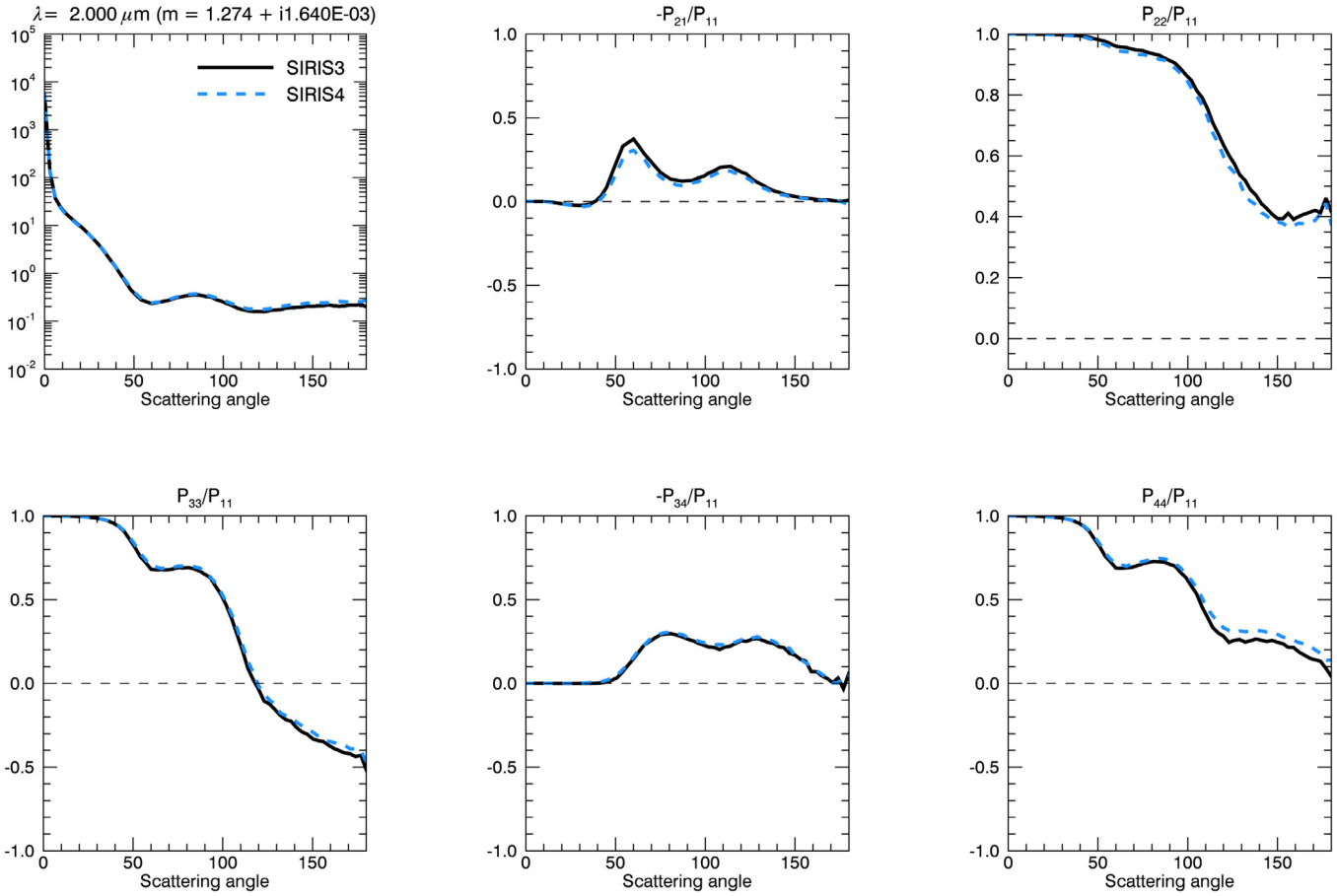

Fig. 6. Angular dependence of scattering by an ensemble of Gaussian-random-sphere ice particles at $\lambda = 2.0$ μm computed with traditional ray optics (SIRIS3) and ray optics with inhomogeneous plane waves (SIRIS4).

homogeneous waves is systematically higher than the ϖ calculated without taking inhomogeneous waves into account. The largest absolute increase was 0.044 at $\lambda = 2.725$ μm, which coincided with the largest relative increase, 6.4%. The differences between the ϖ values computed with SIRIS3 and SIRIS4 are very similar for both hexagonal and Gaussian-random-sphere ice particles. Furthermore, we investigated the changes in the angular-dependent scattering-matrix elements. These are shown for $\lambda = 2.0$ μm in Fig. 6 and for $\lambda = 3.969$ μm in Fig. 7. When compared to the hexagonal ice crystals, the angular-dependent features of the scattering-matrix elements were largely different and smoother overall. However, the differences between SIRIS3 and SIRIS4 results were generally small, largest of them occurring at $\lambda = 1.5$ μm, $\lambda = 2.0$ μm and $\lambda = 3.969$ μm, similarly to the hexagonal ice crystals. Again, when approaching longer wavelengths, scattering is more sensitive to the treatment of inhomogeneous waves (see Fig. 7). P_{22}/P_{11}, P_{33}/P_{11}, and P_{44}/P_{11} are the most sensitive elements, especially at large scattering angles.

Inspired by the similarities in the differences between SIRIS3 and SIRIS4 results for the two particle shapes, we calculated the difference in the single-scattering albedo, $\Delta\varpi = \varpi_{\mathrm{SIRIS4}} - \varpi_{\mathrm{SIRIS3}}$, for each shape and compared it to Im(m). The result in Fig. 8 highlights the Im(m) region of the largest sensitivity to the consideration of inhomogeneous waves in light scattering, almost regardless of particle shape in this case.

5. Conclusions

Ray optics has numerous applications, including single-scattering computations for particles much larger than the wavelength of incident light. For absorbing particles, the waves inside a particle propagate as inhomogeneous plane waves, which has pro-

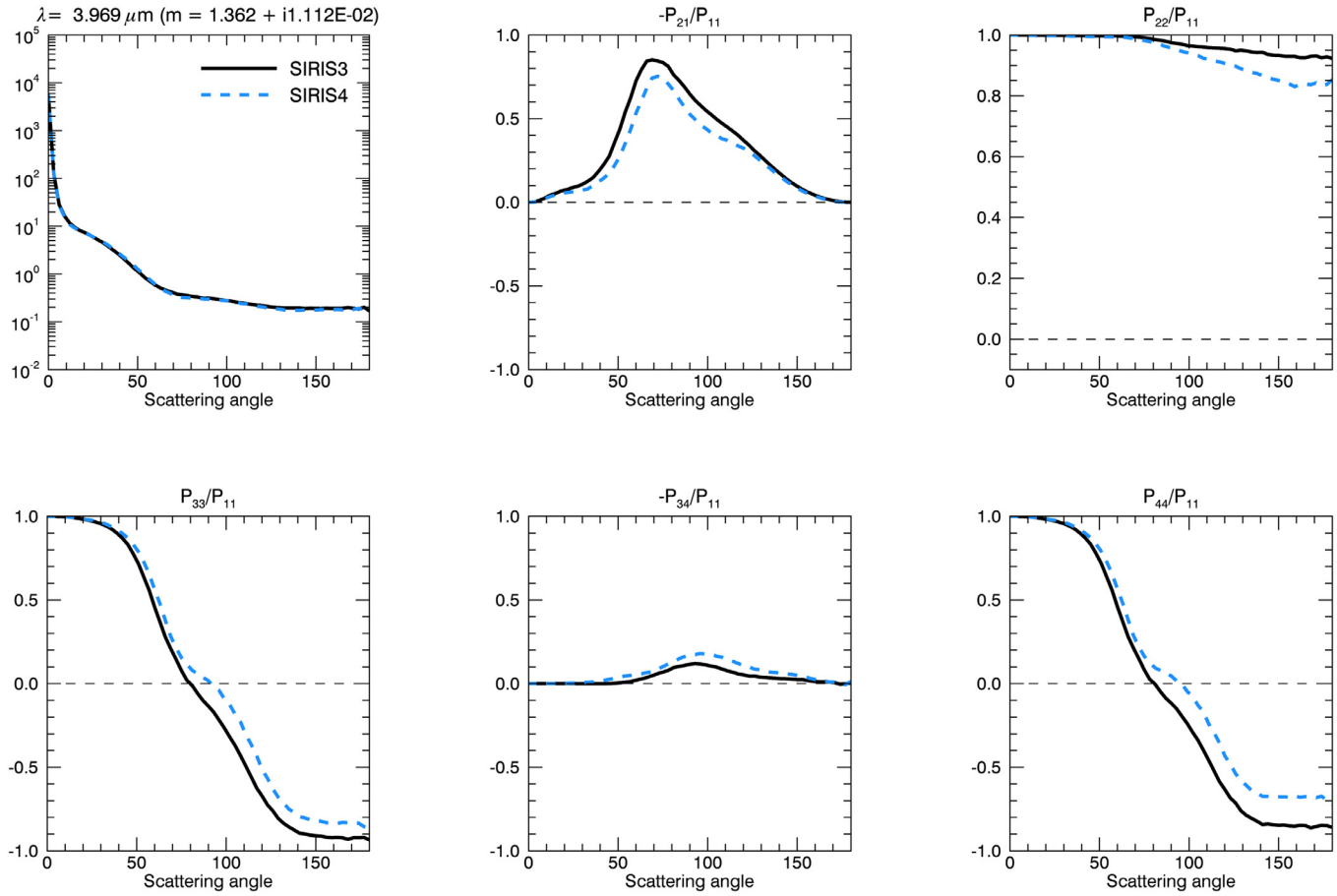

Fig. 7. Angular dependence of scattering by an ensemble of Gaussian-random-sphere ice particles at $\lambda = 3.969$ μm computed with traditional ray optics (SIRIS3) and ray optics with inhomogeneous plane waves (SIRIS4).

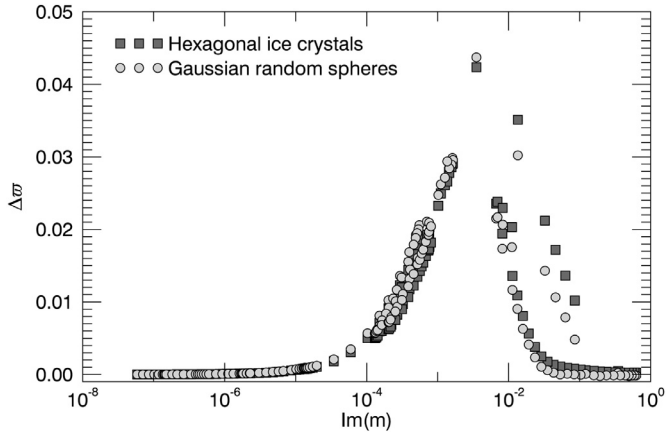

Fig. 8. The dependence of the single-scattering albedo difference, $\Delta\varpi = \varpi_{\mathrm{SIRIS4}} - \varpi_{\mathrm{SIRIS3}}$, on Im($m$) for both hexagonal and Gaussian-random-sphere ice particles.

found consequences to the fundamental concepts of the ray-optics approximation, including the formulation of the Snel and Fresnel equations. In this paper, we have derived the ray-optics solution that takes into account the inhomogeneous nature of the internal waves. We followed the treatment of [33] but expanded it to ray optics in three dimensions, with full 4×4 scattering matrices. We have implemented the solution for the inhomogeneous waves to the ray-optics code SIRIS [18], thus updating it to the version SIRIS4.

For the first evaluations of the magnitude of the inhomogeneous wave correction, we applied SIRIS4 to light scattering by large atmospheric ice crystals in the near-infrared wavelengths from $\lambda = 0.75$ μm to $\lambda = 4.0$ μm. We considered two randomly oriented particle shape ensembles: hexagonal ice crystals and Gaussian-random-sphere ice particles. We discovered a systematic increase in the single-scattering albedo ϖ following the ray-optics formulation based on the inhomogeneous waves. The magnitude of this increase was found to depend on Im(m), and thus, the wavelength of incident light. The largest difference was identified for both shapes at $\lambda = 2.725$ μm, and was $\Delta\varpi = 0.042$ for hexagonal ice crystals and $\Delta\varpi = 0.044$ for Gaussian random spheres. Scattering-matrix elements were found to be generally little affected by the inhomogeneous waves, although some differences were seen at local spectral absorption maxima: the most sensitive elements were P_{22}/P_{11}, P_{33}/P_{11}, and P_{44}/P_{11}, and the effects were the strongest at large scattering angles.

Finally, SIRIS4 was evaluated against the discrete exterior calculus (DEC), which is an exact computational light scattering method. We found that SIRIS4 seems to agree slightly better with the DEC than its preceding version, SIRIS3. This indicates that the inhomogeneous waves are important to consider in scattering by absorbing particles large compared to the wavelength of incident light. Nevertheless, further studies and additional metrics are required to establish the conclusion.

Acknowledgments

H. Lindqvist acknowledges funding from the Academy of Finland, via project number 285421. Research by K. Muinonen, A. Penttilä, J. Räbinä, and J. Martikainen is supported, in part, by the ERC Advanced Grant No. 320773 and the Academy of Finland project number 298137. We also acknowledge the Finnish Ministry of Education and Culture and the CSC — IT center for science for providing the computing resources.

References

[1] Bi L, Yang P, Kattawar GW, Hu Y, Baum BA. Scattering and absorption of light by ice particles: solution by a new physical-geometric optics hybrid method. J Quant Spectrosc Radiat Transfer 2011;112:1492–508.
[2] Borovoi A, A K, N K. The physics-optics approximation and its application to light backscattering by hexagonal ice crystals. J Quant Spectrosc Radiat Transfer 2014;146:181–9.
[3] Wylie DP, Menzel WP. Eight years of high cloud statistics using HIRS. J Clim 1999;12(1):170–84.
[4] Stubenrauch C, Cros S, Guignard A, Lamquin N. A 6-year global cloud climatology from the atmospheric infrared sounder AIRS and a statistical analysis in synergy with CALIPSO and cloudsat. Atmos Chem Phys 2010;10(15):7197–214.
[5] Yang P, Bi L, Baum BA, Liou K-N, Kattawar GW, Mishchenko MI, et al. Spectrally consistent scattering, absorption, and polarization properties of atmospheric ice crystals at wavelengths from 0.2 to 100 µm. J Atmos Sci 2013;70(1):330–47.
[6] Jacobowitz H. A method for computing the transfer of solar radiation through clouds of hexagonal ice crystals. J Quantit Spectrosc Radiat Transfer 1971;11:691–5.
[7] Wendling P, Wendling R, Weickmann HK. Scattering of solar radiation by hexagonal ice crystals. Appl Opt 1979;18:2663–71.
[8] Cai Q, Liou KN. Polarized light scattering by hexagonal ice crystals: theory. Appl Opt 1982;21:3569–80.
[9] Liou KN, Cai Q, Barber PW, Hill SC. Scattering phase matrix comparison for randomly hexagonal cylinders and spheroids. Appl Opt 1983;22:1684–7.
[10] Liou KN, Cai Q, Pollack JB, Cuzzi JN. Light scattering by randomly oriented cubes and parallelepipeds. Appl Opt 1983;22:3001–8.
[11] Takano Y, Jayaweera K. Scattering phase matrix for hexagonal ice crystals computed from ray optics. Appl Opt 1985;24:3254–63.
[12] Muinonen K, Lumme K, Peltoniemi JI, Irvine WM. Light scattering by randomly oriented crystals. Appl Opt 1989;28:3051–60.
[13] Peltoniemi JI, Lumme K, Muinonen K, Irvine WM. Scattering of light by stochastically rough particles. Appl Opt 1989;28:4088–95.
[14] Muinonen K, Nousiainen T, Fast P, Lumme K, Peltoniemi J. Light scattering by Gaussian random particles: ray optics approximation. J Quant Spectrosc Radiat Transfer 1996;55(5):577–601.
[15] Macke A, Müller J, Raschke E. Single scattering properties of atmospheric ice crystals. J Atmos Sci 1996;53:2813–25.
[16] Macke A, Muinonen K. Polarized light scattering at large nonspherical particles. In: Videen Y, Yatskiv, Mishchenko EM, editors. Photopolarimetry in Remote Sensing. Kluwer Academic Publishers, Dordrecht; 2004. p. 45–64.
[17] Grynko Y, Shkuratov Y. Scattering matrix calculated in geometric optics approximation for semitransparent particles faceted with various shapes. J Quant Spectrosc Radiat Transfer 2003;78:319–40.
[18] Muinonen K, Nousiainen T, Lindqvist H, Munoz O, Videen G. Light scattering by Gaussian particles with internal inclusions and roughened surfaces using ray optics. J Quant Spectrosc Radiat Transfer 2009;110:1628–39.
[19] Konoshonkin A, Kustova N, Borovoi A. Beam-splitting code for light scattering by ice crystal particles within geometric-optics approximation. J Quant Spectrosc Radiat Transfer 2015;164:175–83.
[20] Muinonen K. Light scattering by tetrahedral particles in the Kirchhoff approximation. In: T Wriedt E, editor. Electromagnetic and Light Scattering — Theory and Applications VII. Universität Bremen, Germany; 2003. p. 251–4 .
[21] Nousiainen T, Muinonen K. Light scattering by Gaussian, randomly oscillating raindrops. J Quant Spectrosc Radiat Transfer 1999;63:643–66.
[22] Muinonen K, Erkkilä H. Scattering of light by concave-hull-transformed Gaussian particles. In: Videen G, Mishchenko M, Mengüc EMP, Zakharova N, editors. Tenth Conference on Electromagnetic and Light Scattering. Bodrum, Turkey, June 17–22, 2007; 2007. p. 125–8.
[23] Lindqvist H, Muinonen K, Nousiainen T. Light scattering by coated Gaussian and aggregate particles. J Quant Spectrosc Radiat Transfer 2009;110:1398–410.
[24] Virkki A, Muinonen K. Radar scattering by boulders using geometric optics. Planet Space Sci 2015;118:277–84.
[25] Macke A, Mishchenko MI, Cairns B. The influence of inclusions on light scattering by large ice particles. J Geophys Res 1996;101:23311–16.
[26] Nousiainen T, Lindqvist H, McFarquhar GM, Um J. Small irregular ice crystals in tropical cirrus. J Atmos Sci 2011;68(11):2614–27.
[27] Epstein PS. Geometrical optics in absorbing media. Proc Natl Acad Sci 1930;16(1):37–45.
[28] Bohren CF, Huffman DR. Absorption and Scattering of Light by Small Particles. Wiley-VCH Verlag GmbH; 1998. ISBN 9780471293408. doi:10.1002/9783527618156.
[29] Born M, Wolf E. Principles of Optics. Cambridge University Press; 1999. ISBN 9781139644181. doi:10.1017/CBO9781139644181.
[30] Liou KN. An Introduction to Atmospheric Radiation. Academic Press; 2002. ISBN 9780124514515.
[31] Wendisch M, Yang P. Theory of Atmospheric Radiative Transfer. John Wiley & Sons; 2012. ISBN 9783527408368.
[32] Dupertuis M, Acklin B, Proctor M. Generalization of complex Snell–Descartes and Fresnel laws. JOSA A 1994;11(3):1159–66.
[33] Chang PC, Walker J, Hopcraft K. Ray tracing in absorbing media. J Quant Spectrosc Radiat Transfer 2005;96(3):327–41.
[34] Yang P, Gao B-C, Baum BA, Hu YX, Wiscombe WJ, Mishchenko MI, et al. Asymptotic solutions for optical properties of large particles with strong absorption. Appl Opt 2001;40(9):1532–47.
[35] Yang P, Liou K. An "exact" geometric-optics approach for computing the optical properties of large absorbing particles. J Quant Spectrosc Radiat Transfer 2009;110(13):1162–77.
[36] Warren SG, Brandt RE. Optical constants of ice from the ultraviolet to the microwave: a revised compilation. J Geophys Res 2008;113(D14).
[37] Stern A, Tong Y, Desbrun M, Marsden JE. Geometric computational electrodynamics with variational integrators and discrete differential forms. In: Geometry, Mechanics, and Dynamics. Springer; 2015. p. 437–75.
[38] Räbinä J, Mönkölä S, Rossi T. Efficient time integration of Maxwell's equations by generalized finite-differences. SIAM J Sci Comput 2015;37:B834–54.
[39] Räbinä J. On a numerical solution of the Maxwell equations by discrete exterior calculus. Dissertation (Ph.D.). University of Jyväskylä; 2014. http://urn.fi/URN:ISBN:978-951-39-5951-7.
[40] Yee KS. Numerical solution of initial boundary value problems involving Maxwell's equations in isotropic media. IEEE Trans Antennas Propag 1966;14(3):302–7.
[41] Taflove A. Application of the finite-difference time-domain method to sinusoidal steady state electromagnetic penetration problems. IEEE Trans Electromagn Compat 1980;22(3):191–202.
[42] Weiland T. A discretization method for the solution of Maxwell's equations for six-component fields. Electron Commun AEUE 1977;31(3):116–20.
[43] Lindqvist H, Muinonen K, Nousiainen T, Um J, McFarquhar G, Haapanala P, et al. Ice-cloud particle habit classification using principal components. J Geophys Res 2012;117(D16).
[44] Mitchell D, WP A. A model predicting the evolution of ice particle size spectra and radiative properties of cirrus clouds. part ii: dependence of absorption and extinction on ice crystal morphology. J Atmos Sci 1994;51:817–32.
[45] Muinonen K. Introducing the Gaussian shape hypothesis for asteroids and comets. Astron Astrophys 1998;332:1087–98.